PCCP

Accepted Manuscript

ROYAL SOCIETY OF CHEMISTRY

www.rsc.org/pccp

Accelerated Materials Design of $Na_{0.5}Bi_{0.5}TiO_3$ Oxygen Ionic Conductors Based on First Principles Calculations

Xingfeng He, Yifei Mo *

Department of Materials Science and Engineering, University of Maryland, College Park, MD 20742, United States

* yfmo@umd.edu

ABSTRACT

We perform a first principles computational study of designing the $Na_{0.5}Bi_{0.5}TiO_3$ (NBT) perovskite material to increase its oxygen ionic conductivity. In agreement with the previous experiments, our computation results confirm fast oxygen ionic diffusion and good stability of the NBT material. The oxygen diffusion mechanisms in this new material were systematically investigated, and the effects of the local atomistic configurations and dopants on oxygen diffusion were revealed. Novel doping strategies focusing on the Na/Bi sublattice were predicted and demonstrated by the first principles calculations. In particular, the K doped NBT compound achieved good phase stability and an order of magnitude increase in oxygen ionic conductivity of up to 0.1 S/cm at 900K comparing to the prior Mg doped compositions. This study demonstrated the advantages of first principles calculations in understanding the fundamental structure-property relationship and in accelerating the materials design of the ionic conductor materials.

1. INTRODUCTION

Fast oxygen ionic conductor materials have important technological applications in electrochemical devices such as solid oxide fuel cells (SOFCs), oxygen separation membranes and sensors. For example, increasing the oxygen ionic conductivity is critical for increasing the power density and lowering the operational temperature of SOFCs.[1] Over the past decades, significant research efforts have been dedicated to the development of fast oxygen ion conductor materials.[2] Recently, sodium bismuth titanate, $Na_{0.5}Bi_{0.5}TiO_3$ (NBT), a known piezoelectric material, was reported as a new family of oxygen ionic conductor by Li *et al*.[3] In the prior experimental study[3], the NBT material with Mg doping, $Na_{0.5}Bi_{0.49}Ti_{0.98}Mg_{0.02}O_{2.965}$, has achieved an oxygen conductivity of 8 mS/cm at 600 °C,[3] which is comparable to other well-known oxygen ion conductor materials, such as $La_{0.9}Sr_{01}Ga_{0.9}Mg_{0.1}O_{2.9}$ [4] and $Ce_{0.9}Gd_{0.1}O_{1.95}$ [5]. The fast oxygen ion diffusion of the NBT is attributed to the high polarizability of Bi^{3+} cations and is mediated by oxygen vacancies,[3] which are introduced by changing the NBT compositions through Bi deficiency and/or Mg doping[3, 6]. As a newly reported oxygen conductor, this NBT material may potentially achieved even higher oxygen conductivity.

Further improvement of the NBT ionic conductor materials requires the understanding of oxygen diffusion mechanisms in the perovskite crystal structures of the NBT material. The Mg doping has been the only doping methods demonstrated for the NBT material,[3] and the doping of other elements is still to be explored. In particular, the doping at the Na/Bi sites instead of the Ti-site substitutions have not been investigated. Given that the off-stoichiometry of the Na and Bi sites of the perovskites have shown to greatly impact the oxygen diffusion,[3, 6] it is of great interests to understand how the atomic configurations of Na and Bi cations and their substitutions affect the atomistic mechanisms of O diffusion. It has been shown in other pervoskite materials such as $Gd_{0.5}Ba_{0.5}MO_{3-\delta}$ (M=Mn, Co)[7-9] and $PrBaCo_2O_{5+x}$[10] that the cation ordering increases oxygen ionic conductivity. Therefore, gaining the materials insights in the NBT materials are critical for the design and development of this new family of oxygen ion conductors.

The aim of this study is to establish the structure-property relationship of the NBT materials using first principles computation techniques, to understand the O diffusion mechanisms in the NBT material with different cation sublattice or with different doping, and to design the NBT material with improved ionic conductivity on the basis of newly gained materials understanding. We first investigated the phase stability and O diffusion mechanism of the NBT material using

first principles calculations. On the basis of new understanding about this NBT material, we leveraged the first principles calculations to examine a large number of new dopants and to identify the potential dopants that can enhance oxygen diffusion in the NBT material. As a result, new NBT compositions with good phase stability were predicted offering several fold increases in oxygen ionic conductivity. Our study demonstrated the first principles calculation approach in providing materials insights into new materials systems and in designing materials with enhanced properties.

2. METHODS

All density functional theory (DFT) calculations in this study were performed using the Vienna *Ab initio* Simulation package (VASP)[11] within the projector augmented-wave approach.[12] All total energy calculations were performed using the Perdew-Burke-Ernzerhof (PBE) generalized-gradient approximation (GGA) functional.[13] The static DFT calculations were spin-polarized using the convergence parameters consistent with the *Materials Project.*[14-16]

2.1. Site ordering of the NBT materials.

The $Na_{0.5}Bi_{0.5}TiO_3$ (NBT) material has a perovskite crystal structure ABO_3, where Na and Bi ions share the A sites with a disordered co-occupancy and Ti ions occupy the B sites (Fig. S1). The NBT perovskite materials have three phases, such as rhombohedral, tetragonal, and cubic phases.[17] The cubic phase is stabilized at the temperature of 520 °C or higher, and the rhombohedral phase is stabilized at the temperature of 255 °C or lower.[17] The calculations were performed on the cubic phase except for the Nudge-Elastic-Band (NEB) calculations described in 2.4. We used $\left(2\sqrt{2} \times 2\sqrt{2} \times 3\right)$R45° supercell models of the NBT cubic perovskite structure, which contain 24 formula units of $Na_{0.5}Bi_{0.5}TiO_3$ and a total of 120 atoms. We first determined the A-site configurations of Na and Bi ions, which have disordered co-occupancy of the A sites in the NBT perovskite structure. We used the *pymatgen* package [18] to generate a total of 70 symmetrically distinctive structures, of which twenty were generated by minimizing the electrostatic energies of the structures and the other fifty were generated by randomizing the disordered occupancies. All these structures were statically relaxed in the DFT calculations, and the structure of the lowest DFT energy was identified as the ground state structure for other calculations.

2.2. Phase stability

We evaluated the phase stability of the doped NBT compositions using the scheme in ref. [19-21]. Computational phase diagram was constructed using the DFT data of all compounds in the relevant elementary spaces, e.g. Na-Bi-Ti-O, from the *Materials Project*[14, 21, 22] and our calculation results of the NBT compositions. The concept of 'energy above hull' defined in the previous studies[19-21, 23] was used as the measure of the phase stability. The energy above hull ΔE at 0 K is the negative of the reaction energy for the NBT composition to decompose into the predicted equilibrium phases. A positive value of ΔE suggests that the corresponding phase is not thermodynamically stable at 0 K.

To evaluate phase stability of doped NBT at non-zero temperatures, we defined the decomposition energy

$$\Delta G = \Delta E + P\Delta V - T\Delta S \quad (1)$$

at temperature T. Given the purpose of comparing the stability among solid phases, the contribution of the $P\Delta V$ term was small and was neglected as in prior studies,[19-21, 23]. Given the disordering of the A-site Na/Bi cation sublattice, the A-site configurational entropy S_{config} is likely the dominant contribution to ΔS comparing to the configurational contribution of the dopants and the vibrational contribution to the entropy, which were neglected. On the basis of a random mixing of A-site Na and Bi cations at the temperatures of interests, we defined the A-site configuration entropy

$$S_{\text{config}} = -k_{\text{B}}(x \ln(x) + (1-x)\ln(1-x)) \quad (2)$$

where k_{B} was Boltzmann constant, and x was the partial occupancy of Na/Bi at the A sites.

2.3. Chemical stability

We assessed the chemical stability of the NBT materials by constructing oxygen grand potential phase diagrams. Oxygen grand potential phase diagram[19, 20] provided the range of oxygen chemical potential where the NBT was thermodynamically stable. We correlated the O chemical potential to the temperature and O_2 gas partial pressure according to the following equation:

$$\mu_O\left(T, P_{O_2}\right) = \frac{1}{2}\left[E_{O_2} + \Delta H(T, P_{O_2}^0) - TS_{O_2}(T) + k_B T \ln(P_{O_2}/P_{O_2}^0)\right] - \mu_O^0 \quad (3)$$

where E_{O_2} was the DFT energy of O_2 molecules including a correction term of 1.36 eV/O_2 for the GGA errors determined by Wang *et al.*[24] We used the diatomic ideal gas enthalpy $\Delta H(T, P_{O_2}^0) = 7/2\ k_B T$ and the experimental O_2 gas entropy $S_{O_2}(T)$ at 1 atm.[25] The 1/2 term was to account for the two O atoms in the O_2 molecules. The logarithm term described the dependence of the entropy on the oxygen partial pressure based on the ideal gas approximation, where $P_{O_2}^0$ = 1 atm. In this paper, we set the reference $\mu_O^0 = \frac{1}{2}E_{O_2}$, thus $\mu_O = 0\ eV$ at 0 K.

2.4. Diffusion

We performed *ab initio* molecular dynamics (AIMD) simulations to calculate the diffusivity and conductivity of oxygen ions. AIMD simulations were performed on the basis of the Born-Oppenheimer approximation. The DFT-based force evaluations were non-spin-polarized with a minimal Γ-centered 1×1×1 only *k*-point grid. The time step was set to 2 fs. The relaxed ground state structures were used as the initial structures, which were set to an initial temperature of 100 K and were heated to the desired temperatures of 1200 to 2800 K at a constant rate by velocity scaling during 2 ps. AIMD simulations were performed for 60 ps to 700 ps in the NVT ensemble using Nose-Hoover thermostat.[26]

We calculated the mean square displacement (MSD) of each individual oxygen ion as

$$< [r(t)]^2 > = \frac{1}{N}\sum_i < [r_i(t + t_0)]^2 - [r_i(t_0)]^2 > \quad (4)$$

where N was the total number of the O ions and $r_i(t)$ was the displacement of the i-th oxygen ion at the time t. The total MSD was averaged over all oxygen ions and over the time t_0. Every data point of AIMD simulations has a total MSD of more than 700 Å^2.

The diffusion coefficient was defined as the mean square displacement over time:

$$D = \frac{1}{2dt} < [r(t)]^2 > \quad (5)$$

where d = 3 was the dimension of the diffusion system. The value of the diffusion coefficient D was obtained by performing a linear fitting to the relationship of the averaged MSD versus 2dt as in our prior studies.[20, 21, 27] The error bar of diffusivity was the statistical uncertainty in the linear fitting. The calculated D corresponds to self diffusion rather than the combined diffusion of the center of the mass of all oxygen ions. These two definitions of diffusion coefficients become equivalent if there is no cross correlation between the displacement $r_i(t)$ of different particles at

different times. The ionic conductivity σ was estimated according to the Nernst-Einstein relationship.

The nudged elastic band (NEB) calculations were performed in the supercell models of the structures with an oxygen vacancy. We considered the O diffusion pathway along the edge of the TiO_6 octahedra, the only diffusion pathway observed in the AIMD simulations. The migration pathways in the NEB calculations were constructed with seven linearly interpolated images between the fully relaxed starting and ending structures. The energy barrier for oxygen migration was calculated as

$$E_a = E_{\max} - E_{\min},$$

where $E_{\max}$ and $E_{\min}$ were the highest and lowest energy along the migration pathway, respectively. The rhombohedral structure instead of the cubic structure was used in the NEB calculations, which failed to converge in the cubic structures as a result of extensive structural relaxations during the O vacancy migration. Since the rhombohedral structure has the same bonding environment and cation coordination for O ions as the cubic structure, the NEB calculations in the rhombohedral structure are expected to provide the correct trend regarding the effect of local A-site cation configurations on the migration energy barriers.

2.5. Substitution and structure prediction

To investigate the Mg doped NBT material as demonstrated in the previous study,[3] the Mg doped structure, which corresponds to the composition $Na_{0.5}Bi_{0.5}Ti_{0.96}Mg_{0.04}O_{2.96}$, was generated by replacing a Ti atom with Mg and by removing an O atom from the supercell. This composition was chosen to have a similar oxygen vacancy concentration as the experimental composition $Na_{0.5}Bi_{0.49}Ti_{0.98}Mg_{0.02}O_{2.965}$.[3] Other bivalent B^{2+} B-site substitutions, such as $Na_{0.5}Bi_{0.5}Ti_{0.96}B_{0.04}O_{2.96}$, were generated in the same way. We also considered trivalent B^{3+} substitution for B-site Ti by adding an oxygen vacancy and replacing two Ti with B^{3+} in the supercell model, which had the composition $Na_{0.5}Bi_{0.5}Ti_{0.92}B_{0.08}O_{2.96}$. In addition, we considered A^+ and A^{2+} substitutions for A-site Bi. The supercells of these A-site substituted structures had an oxygen vacancy and one or two Bi atoms replaced by A^+ or A^{2+} to form the composition $Na_{0.5}A_{0.04}Bi_{0.46}TiO_{2.96}$ or $Na_{0.5}A_{0.08}Bi_{0.42}TiO_{2.96}$, respectively. The candidate dopants for the NBT material were suggested by the ionic substitution probabilistic model,[28] which was built on the data mining of all known inorganic crystal materials. We only considered the valences of the

dopants that could potentially create oxygen vacancies, while some of the dopants might have multiple possible valences. The valence states of the dopants that were not energetically favorable would be screened and excluded during the phase stability calculations. The configurations of the A-site sublattice, dopants, and oxygen vacancies were determined by the computation methods described in 2.1, and the lowest-energy structures of the doped NBT compositions were identified. The phase stabilities of the doped compositions were calculated using the method described in 2.2, and the doped compounds with good phase stability were identified.

3. RESULTS

3.1.Phase stability of the NBT material

We calculated and compared the DFT energy of all structures with different A-site Na and Bi configurations. The structure with the lowest DFT energy does not exhibit any particular ordering of Na and Bi at the A sites, and a large fraction of structures with different disordered A-site configurations have energies within a range of 20 meV/atom (Fig. S2). We also found the structures with the ordered A-site sublattice with the rock-salt ordering or the layered ordering[29] exhibit higher DFT energies (See Supplementary Information for details). These results indicate a disordered A-site Na/Bi sublattice in the NBT cubic perovskite structure, which is in agreement with the experimental observations.[17, 30]

According to the phase diagram constructed using the DFT results at 0 K, the cubic NBT phase is not thermodynamically stable at 0 K and has an energy above hull ΔE of 18 meV/atom (Table 1). The phase equilibria of the $Na_{0.5}Bi_{0.5}TiO_3$ composition at 0 K are $Na_2Ti_6O_{13}$, $Na_4Ti_5O_{12}$ and Bi_2TiO_5. The computation predicted decomposition phase, $Na_2Ti_6O_{13}$, was observed as a secondary phase in the experiments.[30]

Our calculations show that the cubic phase is thermodynamically stable at high temperatures 1500 K (Table 1) after including the contribution of the configurational entropy of the A-site disordering to the free energy (section 2.3). Therefore, the entropy effect of the A-site disordering plays an important role in stabilizing the cubic perovskite structure of the NBT material. The computation result is consistent with the experimental observation that the NBT cubic structure is a high-temperature phase.[17]

The Mg doping introduces O vacancies in the NBT materials to achieve high oxygen conductivity.[3] We found that Mg doped compound, $Na_{0.5}Bi_{0.5}Ti_{0.96}Mg_{0.04}O_{2.96}$, exhibits a higher value of energy above hull ΔE of 23 meV/atom (Table 1), which is likely caused by the high formation energy of the charge-compensating oxygen vacancies. The value of ΔG is as small as 5 meV/atom at elevated temperatures, such as 1500 K, showing a reasonable phase stability of the doped compound.

Table 1. Phase equilibria and decomposition energies of undoped and Mg-doped NBT materials.

Composition	Phase equilibria at the composition	ΔE at 0 K (meV/atom)	ΔG at 1500 K (meV/atom)
$Na_{0.5}Bi_{0.5}TiO_3$	$Na_2Ti_6O_{13}$, $Na_4Ti_5O_{12}$, Bi_2TiO_5	18	0
$Na_{0.5}Bi_{0.5}Ti_{0.96}Mg_{0.04}O_{2.96}$	$MgTi_2O_5$, Bi_2TiO_5 , $Na_4Ti_5O_{12}$	23	5

3.2. Chemical stability against oxygen

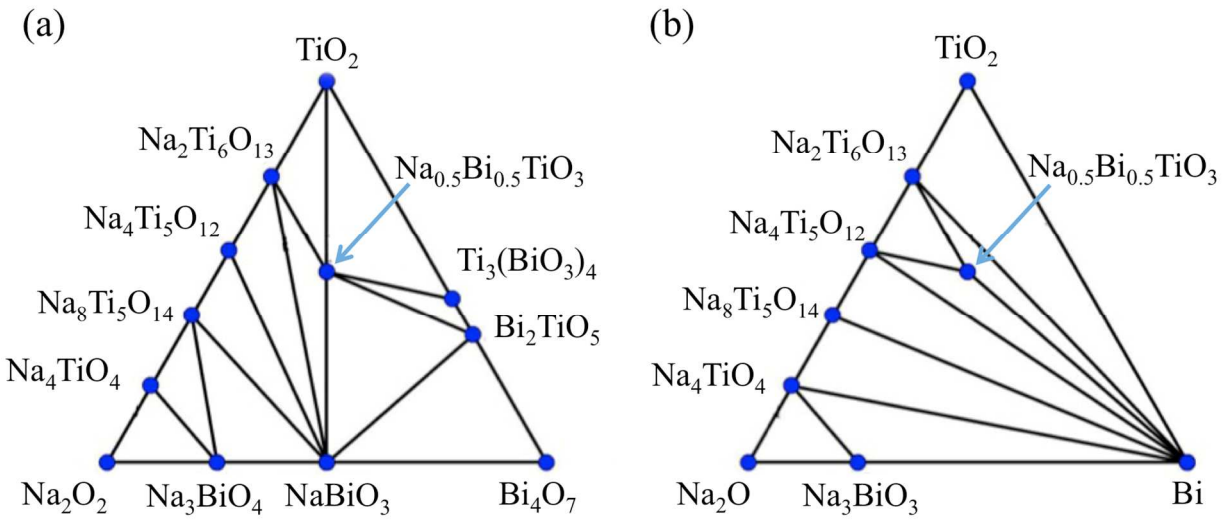

Figure 1. Grand potential phase diagram of Na-Bi-Ti-O at oxygen chemical potential μ_O of (a) -0.60 eV and (b) -2.83 eV.

The chemical stability of a material against oxygen is critical for its application in electrochemical devices such as SOFCs.[1] A good solid electrolyte material in SOFCs needs to sustain the reducing and oxidizing conditions simultaneously at the anode and the cathode. Our

DFT grand potential phase diagrams show that the NBT is stable in a wide range of oxygen chemical potential μ_O from –0.60 eV to –2.83 eV (μ_O = 0 eV at 0K as defined in 2.3). This chemical potential range corresponds to a pressure range from 10^{-3} to 10^{12} Pa of oxygen partial pressure at 1500 K. Our computation results are consistent with the good phase stability of the NBT material in a wide range of O_2 pressure and different chemical environments demonstrated in the experiments.[3]

In addition, we calculated the electronic structures, such as the density of states of the NBT materials (Fig. 2). The DFT calculation predicts a band gap of 2.3 eV for the un-doped NBT, whereas the experimental band gap is 3.26 eV.[31] The large band gap suggests poor electronic conduction in the NBT material. In addition, Mg dopants do not decrease the band gap or induce any defect states in the band gap (Fig. 2b). The computation results are consistent with the relatively low electronic conductivity for both undoped and Mg-doped NBT materials observed in the experiments.

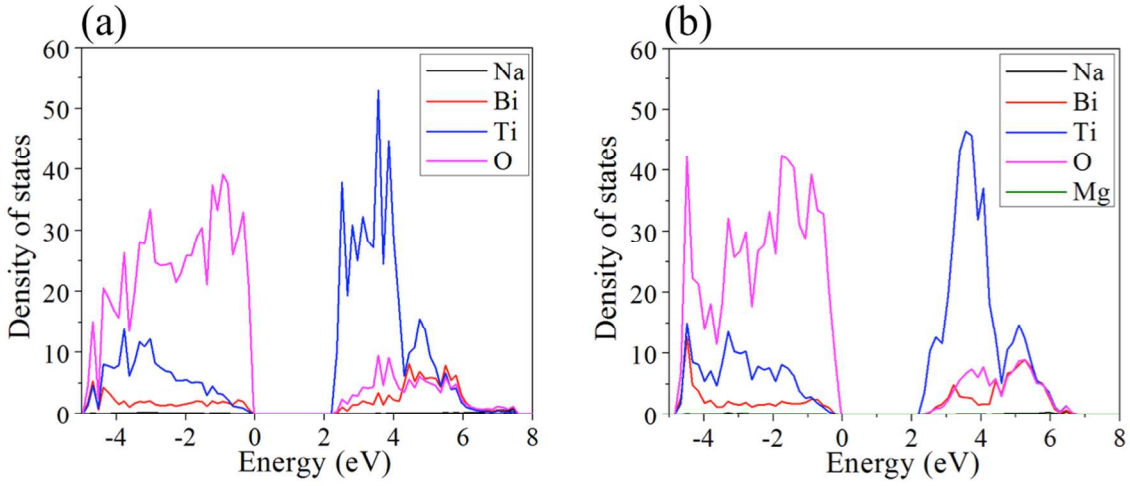

Figure 2. Calculated density of states for (a) $Na_{0.5}Bi_{0.5}TiO_3$, and (b) $Na_{0.5}Bi_{0.5}Ti_{0.96}Mg_{0.04}O_{2.96}$.

3.3. Oxygen ion diffusion in the NBT material

Fast oxygen ion diffusions have been observed in the AIMD simulations of $Na_{0.5}Bi_{0.5}Ti_{0.96}Mg_{0.04}O_{2.96}$. The O^{2-} diffusivity at different temperatures from 1200 K to 2800 K follows an Arrhenius-type relationship (Fig. 3) with an activation energy of 0.61 eV, which is within the range of experimental values from 0.37 to 0.88 eV and is slightly higher than the experimental value of 0.37-0.50 eV for the cubic phase. The extrapolated oxygen diffusivity and

conductivity at 900 K is 2.1×10^{-8} cm^2/s and 8×10^{-3} S/cm, respectively, from the AIMD simulations (Table 2). The AIMD simulation results are in good agreement with the experimental diffusivity of 1.17×10^{-8} cm^2/s at 905 K measured by the tracer diffusion experiments and the ionic conductivity of 8×10^{-3} S/cm measured by impedance spectroscopy at 873 K.[3] The small differences in the diffusional properties are likely caused by the different compositions used in the calculations and in the experiments. For example, comparing to our calculated compound $Na_{0.5}Bi_{0.5}Ti_{0.96}Mg_{0.04}O_{2.96}$, the $Na_{0.5}Bi_{0.49}Ti_{0.98}Mg_{0.02}O_{2.965}$ compound in the experiment has a lower Mg concentration and an additional A-site off-stoichiometry, both of which lower the activation energy for O diffusion as shown later in the NEB calculations and in section 3.4. It is worth noting that the nominal composition is reported in previous experimental study,[3] while our computation uses the exact compositions. In summary, our AIMD simulations confirms the fast O diffusion in the NBT materials and the absence of Na diffusion in agreement with the tracer diffusion experiment.[3]

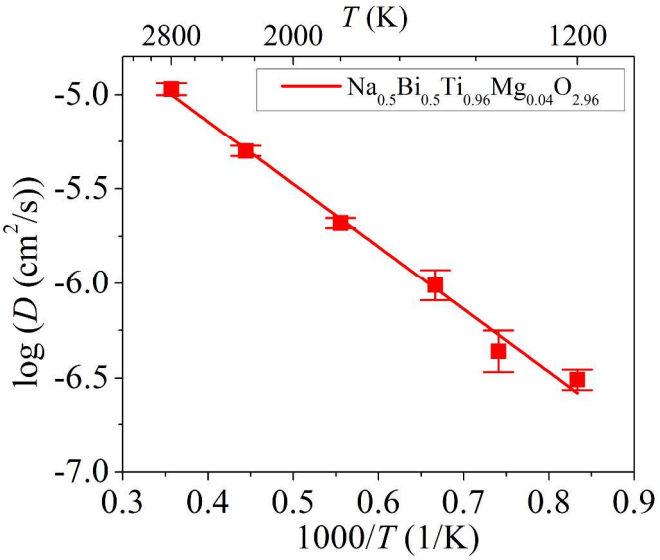

Figure 3. Arrhenius-type plots of O^{2-} diffusion in the $Na_{0.5}Bi_{0.5}Ti_{0.96}Mg_{0.04}O_{2.96}$ from AIMD simulations.

Table 2. Calculated and experimental O^{2-} conductivity σ, diffusivity D, and activation energy E_a of Mg-doped NBT materials.

	σ at ~900 K (mS/cm)	D at ~900 K (10^{-8} cm^2/s)	E_a (eV)
AIMD simulations ($Na_{0.5}Bi_{0.5}Ti_{0.96}Mg_{0.04}O_{2.96}$)	8 ± 3	2.1 ± 0.8	0.66 ± 0.03
Experiments [3] ($Na_{0.5}Bi_{0.49}Ti_{0.98}Mg_{0.02}O_{2.965}$)	8 *	1.17 **	0.37-0.5 (>593 K) 0.84-0.88 (<593 K)

* Ionic conductivity measured by impedance spectroscopy at 600°C [3].
** Oxygen diffusivity measured by tracer diffusion experiments at 632°C [3].

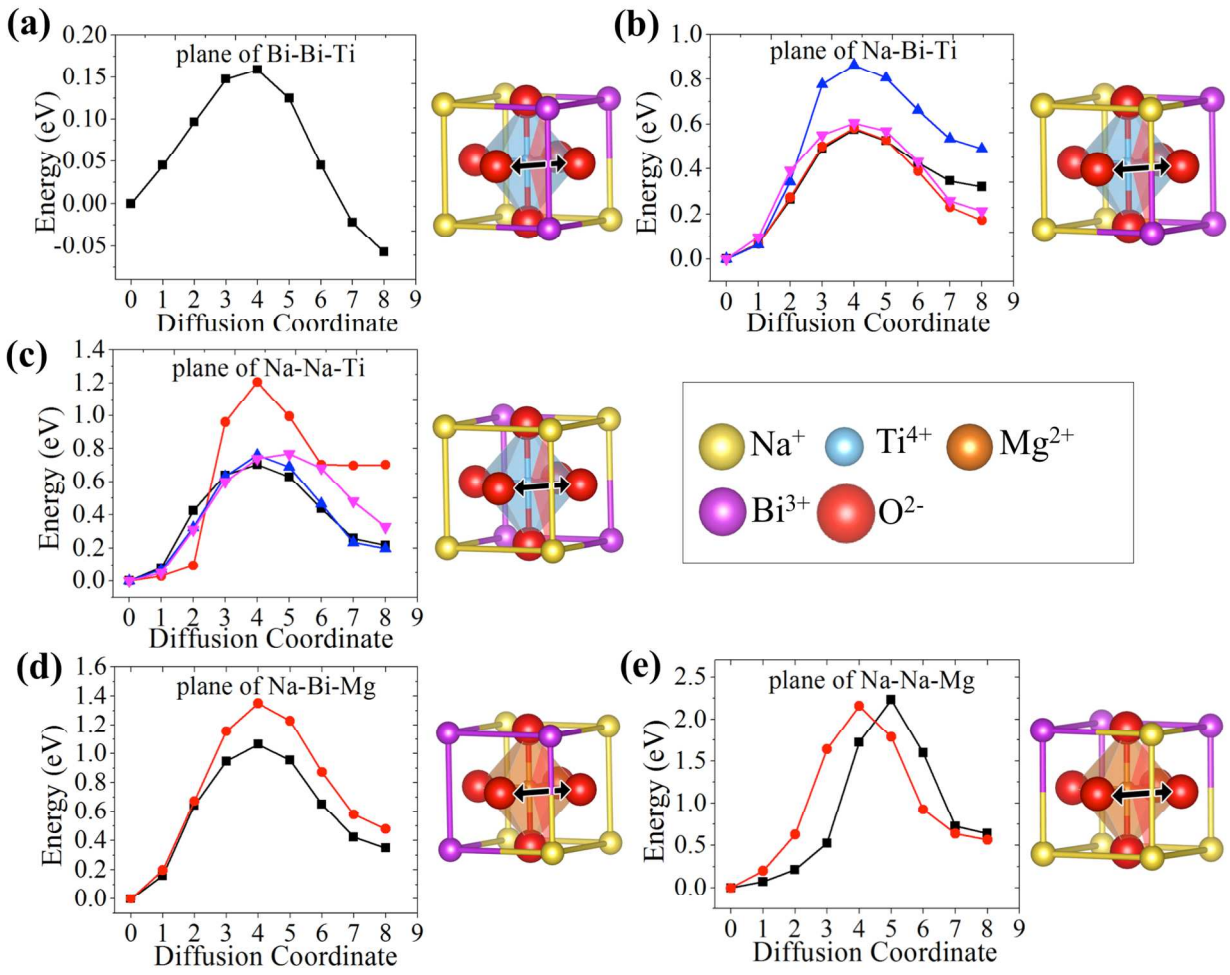

Figure 4. Migration barriers for oxygen vacancies along different diffusion pathways, (a) Bi-Bi-Ti, (b) Na-Bi-Ti, (c) Na-Na-Ti (d) Na-Bi-Mg and (e) Na-Na-Mg. Each diffusion pathway (showing in different colors for clarity) is denoted by the two A-site ions and a B-site ion of the

triangle. The subsets of the cubic perovskite structure on the right illustrate the atomic configuration of different pathways. The A-site ions that are not in the A-A-B triangle may vary in the actual calculations. All oxygen ions on the O sites are shown for clarity.

As observed in the AIMD simulations, the O^{2-} diffusion is mediated by oxygen vacancies migrating along the edge of the TiO_6 octahedra. This oxygen vacancy mechanisms and its diffusion pathway have been previously shown in other perovskite structures in both experiments and computation.[32-36] During the migration, an oxygen vacancy passes through a triangle comprising of two A-site ions and one B-site ion (Figure. 4). We denote the O diffusion pathway by these three atoms A-A-B in the triangle. For example, the Bi-Bi-Ti pathway represents the oxygen migration through a triangle consisting of two A-site Bi ions and one B-site Ti ion (Fig. 4a).

We investigated the oxygen vacancy migration along different diffusion pathways, such as Na-Bi-Ti, Na-Na-Ti, Bi-Bi-Ti, Na-Na-Mg and Na-Bi-Mg (Figure 4), using the Nudged Elastic Band (NEB) methods and found that the migration energy barriers are highly dependent on the different pathways. The oxygen migration along the Bi-Bi-Ti pathway has the lowest energy barrier of 0.22 eV. The Na-Bi-Ti pathway has higher migration energy barriers of 0.6 to 0.85 eV, and the Na-Na-Ti pathway has the highest barriers of 1.0 to 1.3 eV. The values of migration energy barriers vary due to the configurations of the rest of the A-site sublattice. The lower diffusion barriers at the vicinity of Bi atoms for Bi-Bi-Ti and Na-Bi-Ti pathways are likely due to high polarizability of Bi^{3+} ions caused by the $6s^2$ lone-pair electronic structure[1, 5, 37] In the AIMD simulations, most O^{2-} diffusion happened along the Bi-Bi-Ti and Na-Bi-Ti pathways. The oxygen migration along the Na-Bi-Ti pathway is likely the rate-limiting step in the overall oxygen diffusion, and the migration energy for the Na-Bi-Ti pathways of 0.6 eV to 0.85 eV from the NEB calculations is consistent with the activation energy of 0.61 eV from the AIMD simulations.

In addition to the significant impact of local A-site configurations on the O diffusion, the B-site dopants, such as Mg, significantly increase the migration energy barriers for O vacancies. The NEB calculations show that Na-Bi-Mg and Na-Na-Mg pathway have significantly higher migration barriers of 1.0 to 1.3 eV and of 2.1 to 2.2 eV, respectively. The higher migration barrier may be caused by the strong binding between O vacancies and Mg ions at the B sites.

This higher migration barrier at the presence of Mg explains why the activation energy in the AIMD simulations is higher than those in the experiments, which were performed on the composition $Na_{0.5}Bi_{0.49}Ti_{0.98}Mg_{0.02}O_{2.965}$ with a lower Mg concentration.

3.4. Computational prediction of new dopants for the NBT materials

Alternative doping methods are identified to overcome the issue of Mg dopants, which are shown to increase the activation energy of oxygen diffusion (3.3). We aim to identify the doping methods that create oxygen vacancies, increase the oxygen conductivity, and in the meanwhile maintain the phase stability of the material. The substitution probability[28] predicted the following probable dopants for A-site and B-site substitutions, respectively:

B^{2+} =Zn^{2+}, Mn^{2+}, Ni^{2+}, V^{2+}, Mg^{2+}, Hg^{2+}, Co^{2+}, Yb^{2+}, Fe^{2+}, Cd^{2+}, Ca^{2+};

B^{3+}=V^{3+}, Mn^{3+}, Fe^{3+}, Ga^{3+}, Co^{3+}, Cr^{3+}, Al^{3+}, Ti^{3+};

A^{+}= Ag^{+}, Tl^{+}, Na^{+}, K^{+}, Li^{+}, Rb^{+}, Cu^{+}; and

A^{2+}=Yb^{2+}, Pb^{2+}, Sn^{2+}.

We calculated the phase stability for all doped compositions (Fig. 5). The decomposition energies, ΔE and ΔG, provide an indicator for the synthesizability of these doped compositions. Among the $Na_{0.5}Bi_{0.5}Ti_{0.96}B_{0.04}O_{2.96}$ and $Na_{0.5}Bi_{0.5}Ti_{0.92}B_{0.08}O_{2.96}$ generated by the aliovalent B^{2+} and B^{3+} substitution for B-site Ti, respectively (Table 3), the Mg doping exhibits the best phase stability (i.e. the lowest ΔG) as previously demonstrated in the experiment.[3] Other bivalent dopants, Zn, Cd, Hg, and Ni, and trivalent dopants, Fe and V, are predicted as potential dopants for B-site Ti substitution. It is worth noting that Zn and Fe doped NBT has been demonstrated in the experiments,[38, 39] which confirm the predictivity of our first principles computation scheme in predicting potential dopants and in determining the phase stability of doped materials. The Ti^{3+} substitution corresponds to the reduction of B-site Ti^{4+} to Ti^{3+} with oxygen losses. The phase with oxygen loss has poorer phase stability than other doped phases with the same oxygen vacancy concentration. In addition, Fe^{3+} and V^{3+} doping gives better phase stability than their bivalent states. These results show the ability of the calculation in identifying the most energetically favorable valence states for the dopants.

The aliovalent doping of A^{+} and A^{2+} for A-site Bi substitution in the composition $Na_{0.5}A_{0.04}Bi_{0.46}TiO_{2.96}$ and $Na_{0.5}A_{0.08}Bi_{0.42}TiO_{2.96}$ also maintains good phase stability (Table 4 and Fig. 5). For example, the Na and K doped compositions, $Na_{0.54}Bi_{0.46}TiO_{2.96}$ and

$Na_{0.5}K_{0.04}Bi_{0.46}TiO_{2.96}$, have similar decomposition energy comparing to Mg doped $Na_{0.5}Bi_{0.5}Ti_{0.96}Mg_{0.04}O_{2.96}$. The nominal off-stoichiometry compositions, such as Bi deficiency and Na excess, in previous studies[3, 6] may result in a similar effect of the Na substitution for A-site Bi. The good substitution with K is not surprising given that K and Na ions have similar chemistry, and that $K_{0.5}Bi_{0.5}TiO_3$ is known to form a solid solution with NBT.[40-42]

Table 3: Phase equilibria and the decomposition energies for the NBT with B-site Ti substitution.

Dopant ion	Phase equilibria	ΔE at 0 K (meV/atom)	ΔG at 1500 K (meV/atom)
Mg^{2+}	$MgTi_2O_5$, Bi_2TiO_5, $Na_4Ti_5O_{12}$	23	5
Zn^{2+}	Bi_2TiO_5, $Na_4Ti_5O_{12}$, $Na_2Ti_6O_{13}$, ZnO	25	7
Mn^{2+}	Bi_2TiO_5, $Na_4Ti_5O_{12}$, $Na_2Ti_6O_{13}$, $MnTiO_3$	29	11
Ni^{2+}	Bi_2TiO_5, $Na_4Ti_5O_{12}$, $Na_2Ti_6O_{13}$, NiO	26	8
V^{2+}	Bi_2TiO_5, $Na_4Ti_5O_{12}$, $Na_2Ti_6O_{13}$, V_2O_3	30	12
Hg^{2+}	$Na_2Ti_6O_{13}$, Bi_2TiO_5, $Na_4Ti_5O_{12}$,HgO	24	6
Co^{2+}	Bi_2TiO_5, $Na_4Ti_5O_{12}$, $CoTi_2O_5$	33	15
Yb^{2+}	$Na_2Ti_6O_{13}$, Bi_2TiO_5, $Na_4Ti_5O_{12}$,$YbTiO_3$	30	11
Fe^{2+}	Bi_2TiO_5, $Na_4Ti_5O_{12}$, $FeTiO_5$	28	10
Cd^{2+}	Bi_2TiO_5, $Na_4Ti_5O_{12}$, $Na_2Ti_6O_{13}$, $CdTiO_3$	23	5
Ca^{2+}	Bi_2TiO_5 , $Na_4Ti_5O_{12}$, $Na_2Ti_6O_{13}$, $CaTiO_3$	31	13
Pb^{2+}	Bi_2TiO_5, $Na_4Ti_5O_{12}$, $Na_2Ti_6O_{13}$, $PbTiO_3$	43	25
V^{3+}	Bi_2TiO_5, $Na_4Ti_5O_{12}$, $Na_2Ti_6O_{13}$,V_2O_3	24	6
Mn^{3+}	Bi_2TiO_5, $Na_4Ti_5O_{12}$, $Na_2Ti_6O_{13}$, Mn_2BiO_5, Mn_3O_4	28	10
Fe^{3+}	Bi_2TiO_5, $Na_4Ti_5O_{12}$, $Na_2Ti_6O_{13}$, Fe_2O_3	24	6
Ga^{3+}	Bi_2TiO_5, $Na_4Ti_5O_{12}$, $Na_2Ti_6O_{13}$, $NaGaO_2$	26	8
Co^{3+}	Bi_2TiO_5, $Na_4Ti_5O_{12}$, $Na_2Ti_6O_{13}$, Co_3O_4, $NaCo_2O_4$	32	14
Cr^{3+}	Bi_2TiO_5, $Na_4Ti_5O_{12}$, $Na_2Ti_6O_{13}$, $NaCrO_2$	29	11
Al^{3+}	Bi_2TiO_5, $Na_4Ti_5O_{12}$, $Na_2Ti_6O_{13}$, $Al_4Bi_2O_9$	26	8
Ti^{3+}	Bi_2TiO_5, $Na_4Ti_5O_{12}$, $Na_2Ti_6O_{13}$, Bi	34	16

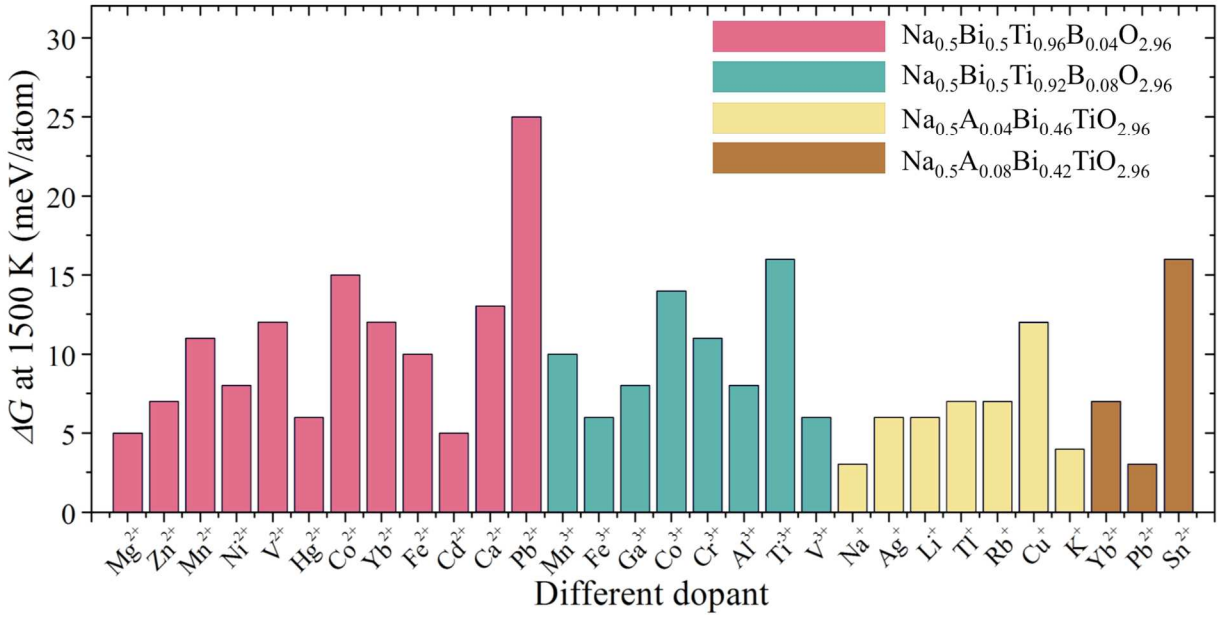

Figure 5. Decomposition energies ΔG at 1500 K for the doped NBT compositions, (from left to right) $Na_{0.5}Bi_{0.5}Ti_{0.96}B_{0.04}O_{2.96}$, $Na_{0.5}Bi_{0.5}Ti_{0.92}B_{0.08}O_{2.96}$, $Na_{0.5}A_{0.04}Bi_{0.46}TiO_{2.96}$, and $Na_{0.5}A_{0.08}Bi_{0.42}TiO_{2.96}$.

Table 4: Phase equilibria and the decomposition energies for the NBT with A-site Bi substitution.

Dopant ion	Phase equilibria	ΔE at 0 K (meV/atom)	ΔG at 1500 K (meV/atom)
Na^+	Bi_2TiO_5, $Na_4Ti_5O_{12}$, $Na_2Ti_6O_{13}$	21	3
Ag^+	Bi_2TiO_5, $Na_4Ti_5O_{12}$, $Na_2Ti_6O_{13}$, Ag_5BiO_4	24	6
Li^+	Bi_2TiO_5, $Na_4Ti_5O_{12}$, $Na_2Ti_6O_{13}$, Li_2TiO_3	24	6
Tl^+	Bi_2TiO_5, $Na_4Ti_5O_{12}$, $Na_2Ti_6O_{13}$, Tl_2TiO_3	25	7
Rb^+	Bi_2TiO_5, $Na_4Ti_5O_{12}$, $Na_2Ti_6O_{13}$, $Rb_2Ti_6O_{13}$	25	7
Cu^+	Bi_2TiO_5, $Na_4Ti_5O_{12}$, $Na_2Ti_6O_{13}$, Cu_2O	30	12
K^+	Bi_2TiO_5, $Na_4Ti_5O_{12}$, $K_2Ti_6O_{13}$, $Na_2Ti_6O_{13}$	22	4
Yb^{2+}	Bi_2TiO_5, $Na_4Ti_5O_{12}$, $Na_2Ti_6O_{13}$, $YbTiO_3$	25	7
Pb^{2+}	Bi_2TiO_5, $Na_4Ti_5O_{12}$, $Na_2Ti_6O_{13}$, $PbTiO_3$	21	3
Sn^{2+}	Bi_2TiO_5, $Na_4Ti_5O_{12}$, $Na_2Ti_6O_{13}$, $Sn_2Bi_2O_7$, Bi	34	16

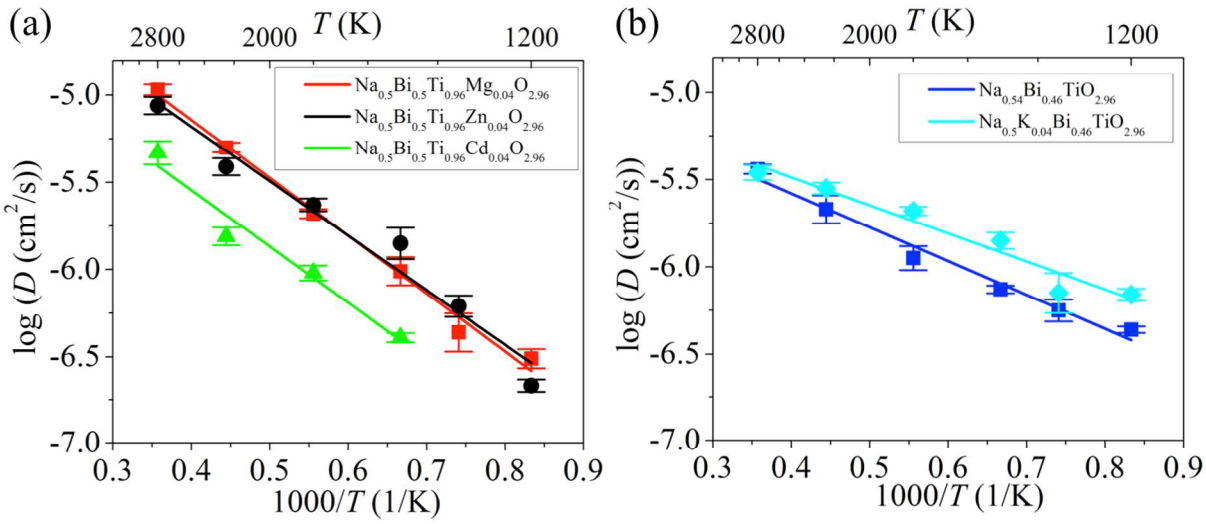

Figure 6. Arrhenius-type plots of the diffusivity of (a) $Na_{0.5}Bi_{0.5}Ti_{0.96}B_{0.04}O_{2.96}$ (B=Mg, Zn, Cd) and (b) $Na_{0.54}Bi_{0.46}TiO_{2.96}$ and $Na_{0.5}K_{0.04}Bi_{0.46}TiO_{2.96}$.

Table 5. Diffusional properties of doped NBT materials. Error bound of the ionic conductivity is estimated based on the error bars of E_a and D obtained during the linear fitting.

Composition	E_a (eV)	σ at 900 K (mS/cm)	Error bound $[\sigma_{min}, \sigma_{max}]$ (mS/cm)
$Na_{0.5}Bi_{0.5}Ti_{0.96}Mg_{0.04}O_{2.96}$	0.66 ± 0.03	8	[5, 12]
$Na_{0.5}Bi_{0.5}Ti_{0.96}Zn_{0.04}O_{2.96}$	0.62 ± 0.06	13	[5, 31]
$Na_{0.5}Bi_{0.5}Ti_{0.96}Cd_{0.04}O_{2.96}$	0.64 ± 0.09	6	[2, 23]
$Na_{0.54}Bi_{0.46}TiO_{2.96}$	0.38 ± 0.03	30	[20, 46]
$Na_{0.5}K_{0.04}Bi_{0.46}TiO_{2.96}$	0.32 ± 0.04	96	[56, 164]

The doped compounds with good phase stability were further evaluated for their oxygen diffusional properties. We performed AIMD simulations of $Na_{0.5}Bi_{0.5}Ti_{0.96}Zn_{0.04}O_{2.96}$ and $Na_{0.5}Bi_{0.5}Ti_{0.96}Cd_{0.04}O_{2.96}$ to evaluate their diffusional properties. The Zn-doped NBT shows similar O^{2-} conductivity (13 mS/cm at 900K) and activation energy (0.62 eV) comparing to Mg doping, while the Cd-doped NBT has a lower O^{2-} conductivity of 6 mS/cm at 900 K (Fig. 6 and Table 5). Therefore, Zn or Cd doping does not address the problems of Mg dopants in increasing oxygen migration barrier.

The NBT materials with A-site doping such as $Na_{0.54}Bi_{0.46}TiO_{2.96}$ and $Na_{0.5}K_{0.04}Bi_{0.46}TiO_{2.96}$ exhibit improved diffusional properties comparing to those with B-site doping. Our AIMD simulations predict that the $Na_{0.54}Bi_{0.46}TiO_{2.96}$ compound has an activation energy of 0.38 eV and an ionic conductivity of 30 mS/cm at 900 K. The K doped compound $Na_{0.5}K_{0.04}Bi_{0.46}TiO_{2.96}$ has an even lower activation energy of 0.32 eV and the highest conductivity of 96 mS/cm at 900 K,

which is an order of magnitude higher than the Mg-doped $Na_{0.5}Bi_{0.5}Ti_{0.96}Mg_{0.04}O_{2.96}$ at the same oxygen vacancy concentration. The A-site doping of the NBT material system overcomes the binding issue between O vacancies and B-site dopants (e.g. Mg) and provides a significant improvement in oxygen ionic conductivity.

3.5. Effect of cation sublattice ordering

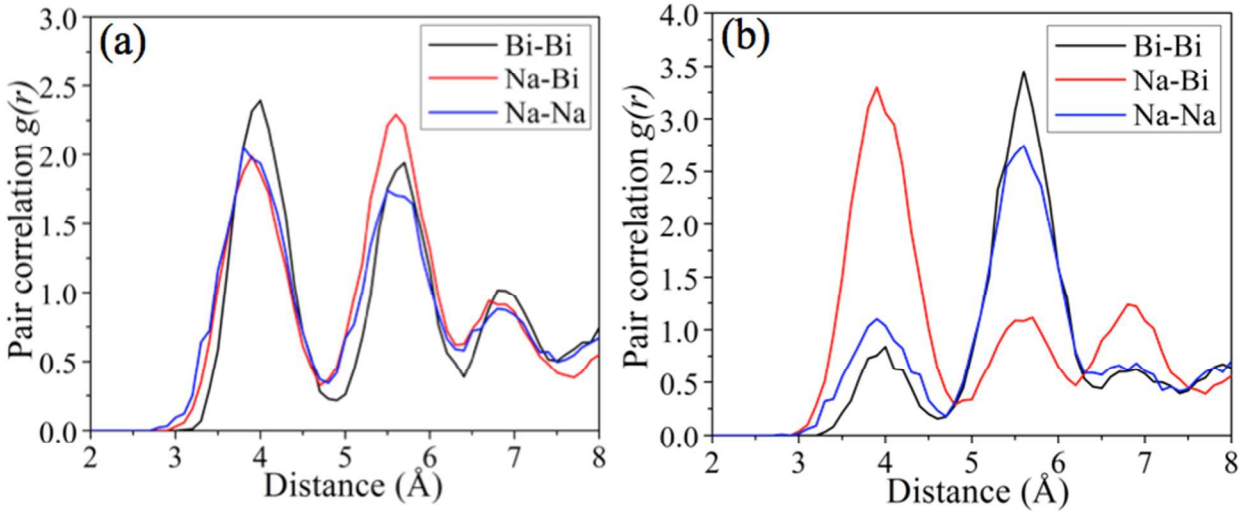

Figure 7. Pair correlation function $g(r)$ of (a) a disordered A-site Na/Bi sublattice and (b) a relatively ordered A-site Na/Bi sublattice in the $Na_{0.54}Bi_{0.46}TiO_{2.96}$, respectively.

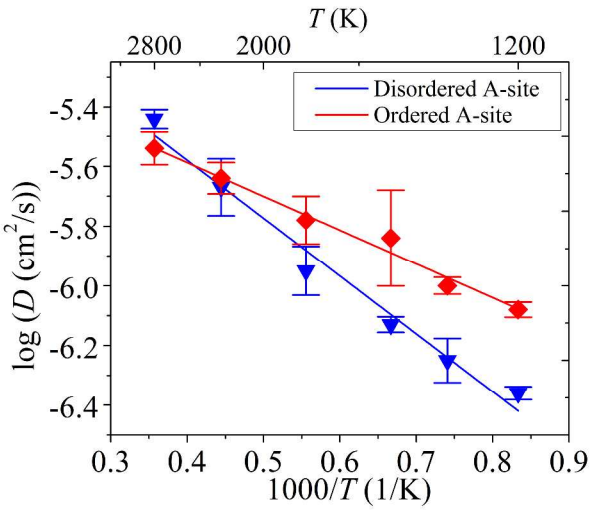

Figure 8. Arrhenius-type plots of oxygen diffusivity in $Na_{0.54}Bi_{0.46}TiO_{2.96}$ with disordered (blue) and ordered (red) A-site cation sublattice.

Given that the oxygen vacancy migration energy barriers is strongly dependent on the local Na/Bi A-site configurations (section 3.3), the oxygen ionic conductivity in the NBT materials may depend on the specific ordering of the A-site Na/Bi cation sublattices. To investigate the dependence of ionic conductivity on the A-site ordering in the NBT, we generated a hypothetical structure of $Na_{0.54}Bi_{0.46}TiO_{2.96}$ with an A-site Na/Bi sublattice that has a nearly rock-salt ordering.[29] In this rock-salt ordered A-site sublattice, most Na ions are nearest neighbors with Bi ions showing by the predominant first peak of Na-Bi at ~4 Å (Fig. 7b). The small occurrence of the first Na-Na and Bi-Bi peaks is due to the A-site off-stoichiometry and the symmetry incompatibility between the rock-salt ordering and the supercell lattice. The structure with the disordered Na/Bi sublattice has similar peak intensities for the Na-Bi, Na-Na, and Bi-Bi (Fig. 7a) nearest neighbors. This A-site disordered structure is the lowest energy structure of this composition, which has a formation energy of 27 meV/atom lower than the structure with ordered A-site sublattice.

A significant enhancement of the O^{2-} diffusion is observed in the structure with ordered A-site sublattice (Fig. 8). Comparing to the disordered A-site NBT, the O^{2-} conductivity extrapolated at 900 K is increased from 0.03 S/cm to 0.15 S/cm, and the activation energy is decreased from 0.38 eV to 0.24 eV (Fig. 8). Therefore, ordering the cation sublattice, as a potential design strategy, improves O^{2-} conductivity in the NBT materials.

DISCUSSION

Our first principles computation results about the oxygen ionic conductivity, diffusivity, and activation energy of the NBT materials are in good agreement with the previous experimental reports by Li *et al.*[3, 6] This agreement demonstrated the validity of the computation scheme. Our computation revealed the strong dependence of the oxygen vacancy migration barrier on the nearest-neighbor cations at A sites and B sites of the perovskite structure. In particular, as a critical problem for the fast oxygen diffusion, the B-site substitution dopants, such as Mg, increase the oxygen vacancy migration barriers. According to our first principles computation results on a large number of B-site doped NBT materials, this high oxygen migration barrier is intrinsic for B-site substitutions, which bind with oxygen vacancies, and cannot be mitigated by using other dopants, such as Zn or Cd.

Our first principles computation predicted a more promising material design strategy based on the A-site substitutions to resolve the problem of the B-site substitutions. We demonstrated the A-site substitutions using a variety of dopants with reasonable phase stability in computation. In particular, the NBT compositions with the Na or K doping have shown good phase stability and high oxygen ionic conductivity. For example, the $Na_{0.54}Bi_{0.46}TiO_{2.96}$ and $Na_{0.5}K_{0.04}Bi_{0.46}TiO_{2.96}$ have similar phase stability and a significant increase in ionic conductivity, which is predicted to be 30 mS/cm and 96 mS/cm at 900K, respectively, comparing to the $Na_{0.5}Bi_{0.5}Ti_{0.96}Mg_{0.04}O_{2.96}$ at the same oxygen vacancy concentration. The improvement in the Na and K doped NBT materials is likely due to the disordered A-site sublattice of Na and Bi ions. This disordered A-site sublattice can form different local atomistic configurations to accommodate the electrostatic and strain fields of the dopants, which helps to maintain the phase stability of the doped structures and to reduce the undesired binding with B-site dopants. Our computation results of A-site doping are consistent with a recent report[6] showing the strong effects of A-site off-stoichiometry on electronic and ionic conduction, though a direct comparison between these two studies is difficult as nominal compositions were used in previous experiments.[3, 6]

The computationally predicted doping methods and compositions are to be verified in experimental studies. The computational results for both phase stability and diffusional properties are based on the doped compositions with the oxygen vacancy concentration of 1.39% (one vacancy out of 72 oxygen sites). It is difficult to access lower doping concentrations, which require supercells with larger sizes. Even if the specific oxygen vacancy concentration were not achieved in the experiments, our predicted doping methods still provide correct trend for increasing ionic conductivity. In addition, we did not consider the formation of competing defects, such as planar defects, anti-site defects and segregations, in the doped compositions. Though these defects may potentially form to lower the oxygen vacancy concentration in the material, the computationally predicted compositions with decent phase stability are expected to be synthesizable and to provide decent ionic conductivity.

In addition, we demonstrated the design strategy of ordering the A-site cation sublattice to increase oxygen diffusion in the NBT materials. The AIMD simulations predicted that the ordered A-site sublattice provided a higher O^{2-} conductivity and a lower activation energy. The different A-site sublattices in these two structures lead to different local pathways for O diffusion

and different overall O percolation networks. The O diffusion in the structure with ordered A-site sublattice is dominated by Na-Bi-Ti diffusion pathways, while all Na-Bi-Ti, Bi-Bi-Ti, and Na-Bi-Ti pathways are present in the disordered structure. However, the poorer O^{2-} diffusion in the disordered A-site sublattice cannot be explained by the higher fraction of the low-barrier Bi-Bi-Ti diffusion pathways. We speculate that the ordered cation sublattice makes a homogenous energy land scape for oxygen migrations, where the local trapping of oxygen ions is inhibited.[43] Unfortunately, the higher formation energy of the ordered A-site lattice may impede the realization of the NBT structures with ordered A-site sublattice.

This study demonstrated how one can use first principles calculation methods to understand the limitations in a new material system and to overcome these limitations by designing the materials. The first principles computation identified promising dopants out of all possible elements, and determined whether the doped phases are stable and whether they provide enhanced properties. The materials design capabilities rely on accurate calculations of materials properties,[20, 21, 27] an algorithm to predict new dopants and substitutions,[28] and an infrastructure, such as the *Materials Project*,[14] to assess the phase stability of new compounds and structures. The first principles computation design is scalable and can be performed in a highly parallel and rapid fashion to predict new materials with enhanced properties. The materials design workflow demonstrated in this study is not limited to oxygen ionic conductor materials, and can be easily transferred to other (e.g. Li^+, Na^+) ionic conductor materials.

CONCLUSION

In summary, we performed a first principles study of the phase stability, chemical stability, and diffusion mechanisms of the NBT oxygen ion conductor materials. The computation results were in good agreement with previous experiments[3]. Our calculations confirm that the oxygen conduction is mediated by oxygen vacancies, and that the local atomistic configurations have a significant impact on the oxygen diffusion. While the high polarizability of the Bi ions promotes fast O diffusion, the Mg dopants bind with oxygen vacancies and increase the oxygen migration barriers. This fundamental limitation of the Mg dopants motivated the first principles computational design to identify new doped NBT materials. Our first principles computation predicted that Zn and Cd dopants at B sites did not improve the oxygen ionic conductivity, and

that Na and K were promising dopants to increase oxygen ionic conductivity. The newly designed NBT materials with A-site Na and K substituted A sites exhibited a many-fold increase in the ionic conductivity at 900K comparing to that in the Mg doped compound at the same oxygen vacancy concentration. This study demonstrated that the NBT material system is promising as fast oxygen ionic conductors, and that first principles computation has the ability to significantly accelerate the materials design processes.

Acknowledgement

This work was partially supported by Office of Naval Research (ONR) under award No. N00014-14-1-0721. This research used computational resources from the University of Maryland supercomputing resources and from the Extreme Science and Engineering Discovery Environment (XSEDE), which was supported by National Science Foundation grant number TG-DMR130142.

References

1. E. D. Wachsman and K. T. Lee, *Science*, 2011, **334**, 935-939.
2. S. J. Skinner and J. A. Kilner, *Materials Today*, 2003, **6**, 30-37.
3. M. Li, M. J. Pietrowski, R. A. De Souza, H. Zhang, I. M. Reaney, S. N. Cook, J. A. Kilner and D. C. Sinclair, *Nat. Mater.*, 2014, **13**, 31-35.
4. C. Haavik, E. M. Ottesen, K. Nomura, J. A. Kilner and T. Norby, *Solid State Ionics*, 2004, **174**, 233-243.
5. D. W. Jung, K. L. Duncan and E. D. Wachsman, *Acta Mater.*, 2010, **58**, 355-363.
6. M. Li, H. Zhang, S. N. Cook, L. Li, J. A. Kilner, I. M. Reaney and D. C. Sinclair, *Chem. Mater.*, 2015, **27**, 629-634.
7. A. Taskin, A. Lavrov and Y. Ando, *Appl. Phys. Lett.*, 2005, **86**, 091910.
8. J. Hermet, G. Geneste and G. Dezanneau, *Appl. Phys. Lett.*, 2010, **97**, 174102.
9. D. Parfitt, A. Chroneos, A. Tarancón and J. A. Kilner, *J. Mater. Chem.*, 2011, **21**, 2183-2186.
10. G. Kim, S. Wang, A. Jacobson, L. Reimus, P. Brodersen and C. Mims, *J. Mater. Chem.*, 2007, **17**, 2500-2505.
11. G. Kresse and J. Furthmuller, *Phys. Rev. B.*, 1996, **54**, 11169-11186.
12. P. E. Blöchl, *Phys. Rev. B.*, 1994, **50**, 17953-17979.
13. J. P. Perdew, M. Ernzerhof and K. Burke, *J. Chem. Phys.*, 1996, **105**, 9982-9985.
14. A. Jain, S. P. Ong, G. Hautier, W. Chen, W. D. Richards, S. Dacek, S. Cholia, D. Gunter, D. Skinner, G. Ceder and K. A. Persson, *Apl Mater*, 2013, **1**, 011002.
15. A. Jain, G. Hautier, C. J. Moore, S. Ping Ong, C. C. Fischer, T. Mueller, K. A. Persson and G. Ceder, *Comput. Mater. Sci.*, 2011, **50**, 2295-2310.

16. A. Jain, G. Hautier, S. P. Ong, C. J. Moore, C. C. Fischer, K. A. Persson and G. Ceder, *Phys. Rev. B.*, 2011, **84**, 045115.
17. G. Jones and P. Thomas, *Acta Crystallogr. Sect. B: Struct. Sci.*, 2002, **58**, 168-178.
18. S. P. Ong, W. D. Richards, A. Jain, G. Hautier, M. Kocher, S. Cholia, D. Gunter, V. L. Chevrier, K. A. Persson and G. Ceder, *Comput. Mater. Sci.*, 2013, **68**, 314-319.
19. S. P. Ong, L. Wang, B. Kang and G. Ceder, *Chem. Mater.*, 2008, **20**, 1798-1807.
20. Y. Mo, S. P. Ong and G. Ceder, *Chem. Mater.*, 2011, **24**, 15-17.
21. S. P. Ong, Y. Mo, W. D. Richards, L. Miara, H. S. Lee and G. Ceder, *Energy Environ. Sci.*, 2013, **6**, 148-156.
22. S. P. Ong, A. Jain, G. Hautier, B. Kang and G. Ceder, *Electrochem. Commun.*, 2010, **12**, 427-430.
23. S. P. Ong, L. Wang, B. Kang and G. Ceder, *Chem. Mater.*, 2008, **20**, 1798-1807.
24. L. Wang, T. Maxisch and G. Ceder, *Phys. Rev. B.*, 2006, **73**, 195107.
25. M. W. Chase, *NIST-JANAF thermochemical tables*, American Chemical Society ; American Institute of Physics for the National Institute of Standards and Technology: Washington, DC1998.
26. S. Nose, *Prog. Theor. Phys. Suppl.*, 1991, **103**, 1-46.
27. Y. Mo, S. P. Ong and G. Ceder, *Chem. Mater.*, 2014, **26**, 5208-5214.
28. G. Hautier, C. Fischer, V. Ehrlacher, A. Jain and G. Ceder, *lnorg. Chem.*, 2010, **50**, 656-663.
29. B. Burton and E. Cockayne, *AIP Conf. Proc.*, 2001, **582**, 82-90.
30. I. Levin and I. M. Reaney, *Adv. Funct. Mater.*, 2012, **22**, 3445-3452.
31. M. Bousquet, J.-R. Duclère, E. Orhan, A. Boulle, C. Bachelet and C. Champeaux, *J. Appl. Phys.*, 2010, **107**, 104107.
32. M. Yashima, M. Itoh, Y. Inaguma and Y. Morii, *J. Am. Chem. Soc.*, 2005, **127**, 3491-3495.
33. M. Yashima and T. Tsuji, *J. Appl. Crystallogr.*, 2007, **40**, 1166-1168.
34. M. Yashima and T. Kamioka, *Solid State Ionics*, 2008, **178**, 1939-1943.
35. M. S. Islam, *J. Mater. Chem.*, 2000, **10**, 1027-1038.
36. T. Mayeshiba and D. Morgan, *Phys. Chem. Chem. Phys.*, 2015, **17**, 2715-2721.
37. D. S. Aidhy, S. B. Sinnott, E. D. Wachsman and S. R. Phillpot, *Ionics*, 2010, **16**, 297-303.
38. C.-S. Chou, C.-Y. Wu, R.-Y. Yang and C.-Y. Ho, *Adv. Powder Technol.*, 2012, **23**, 358-365.
39. C. H. Yang, G. D. Hu, W. B. Wu, H. T. Wu, F. Yang, Z. Y. Lu and L. Wang, *Appl. Phys. Lett.*, 2012, **100**, 022909.
40. J. Kreisel, A. Glazer, G. Jones, P. Thomas, L. Abello and G. Lucazeau, *J. Phys.: Condens. Matter*, 2000, **12**, 3267-3280.
41. O. Elkechai, M. Manier and J. P. Mercurio, *Phys. Status Solidi*, 1996, **157**, 499-506.
42. S. Zhao, G. Li, A. Ding, T. Wang and Q. Yin, *J. Phys. D: Appl. Phys.*, 2006, **39**, 2277-2281.
43. T. Norby, *J. Mater. Chem.*, 2001, **11**, 11-18.